PHYSICAL REVIEW B VOLUME 40, NUMBER 4 1 AUGUST 1989

Structure of the interstitial oxygen defect in $La_2NiO_{4+\delta}$

J. D. Jorgensen, B. Dabrowski, Shiyou Pei, D. R. Richards, and D. G. Hinks
Materials Science Division, Argonne National Laboratory, Argonne, Illinois 60439
(Received 28 February 1989)

Using Rietveld refinement of neutron powder diffraction data, we show that the excess oxygen in $La_2NiO_{4+\delta}$ ($0.13<\delta<0.18$) is incorporated as an interstitial oxygen defect. The defect is located near the $(\frac{1}{4},\frac{1}{4},\frac{1}{4})$ site in the orthorhombic *Fmmm* structure, which provides a favorable coordination to four La atoms but requires four nearby oxygen atoms to be displaced from their normal positions. The defect concentration determined from structural refinement agrees well with the overall oxygen stoichiometry determined by hydrogen reduction. For intermediate oxygen contents ($\delta\approx0.07$) the system separates into two phases with different defect concentrations. Structural data suggest that the nearly stoichiometric phase, $0<\delta<0.02$, incorporates excess oxygen by forming a different defect. Except for large differences in the solubility of the oxygen defect, $La_2NiO_{4+\delta}$ exhibits behavior remarkably similar to superconducting $La_2CuO_{4+\delta}$, suggesting that the oxygen defect structures are the same in both systems.

INTRODUCTION

It has recently been shown that in superconducting $La_2CuO_{4+\delta}$ excess lattice oxygen is the doping mechanism responsible for metallic behavior.[1] In that system, the excess oxygen is usually incorporated by annealing in high-pressure oxygen at temperatures near 500 °C.[2,3] Since the solubility for the excess oxygen defect is rather low (typical values are $\delta<0.05$ for oxygen pressures below 3 kbar), detailed studies of the structure and behavior of this defect have been hampered by difficulties in sample preparation. Samples made in oxygen pressures below 3 kbar are, in fact, two-phase mixtures of an oxygen-rich superconducting phase and a nearly stoichiometric (i.e., $\delta\approx0$) nonsuperconducting phase with almost identical structures.[1] This phase separation suggests a miscibility gap in the oxygen-concentration phase diagram and implies that much higher oxygen pressures are required to synthesize single-phase samples of superconducting $La_2CuO_{4+\delta}$.

As an alternative approach to studying the structure and behavior of the excess-oxygen defect, we have synthesized and examined samples of the isostructural compound $La_2NiO_{4+\delta}$. It has been known for a number of years that $La_2NiO_{4+\delta}$ exhibits a wide range of oxygen stoichiometry. A review of the work on $La_2NiO_{4+\delta}$ has recently been given by Buttrey *et al.*[4] In the earlier literature, this nonstoichiometry was usually attributed to the presence of Ruddlesden-Popper phase intergrowths or deviations in the metal-ion ratio (i.e., metal site vacancies). However, more recent work has conclusively shown that the observed nonstoichiometry cannot be attributed to the presence of intergrowth phases or deviations in the metal-atom ratio[5] and that the system can, in fact, accommodate a large concentration ($0<\delta<0.2$) of excess lattice oxygen.[4]

These reports of a large amount of excess lattice oxygen in $La_2NiO_{4+\delta}$ led us to believe that the behavior was similar to that observed in $La_2CuO_{4+\delta}$ except that the former compound exhibited a greater solubility for the oxygen defect. Because of this, we were hopeful that in the $La_2NiO_{4+\delta}$ system it would be possible to synthesize single-phase samples with excess oxygen that could be used to learn the structure of the oxygen defect by neutron powder diffraction. In this paper we show that, indeed, single-phase samples with $\delta=0.18$ can readily be synthesized in 1 atm. of oxygen, and we report the structure of the oxygen defect. Although it is not the purpose of this paper to fully investigate the oxygen composition phase diagram of $La_2NiO_{4+\delta}$, we also show that at lower oxygen concentrations ($\delta\approx0.07$) a sample made by the same technique is separated into two phases, $\delta\approx0.02$ and 0.13, due to a miscibility gap in the oxygen-concentration phase diagram. This observation suggests an overall phase behavior similar to that observed for $La_2CuO_{4+\delta}$,[1] and gives us some confidence in speculating that the excess-oxygen defects in these two systems have similar structures. Our results for the structure of the interstitial oxygen defect take on added significance in light of the recent announcement of traces of superconductivity in the $La_{2-x}Sr_xNiO_{4+\delta}$ system.[6]

SAMPLE PREPARATION

A 15-g powder sample of $La_2NiO_{4+\delta}$ was synthesized from stoichiometric mixtures of the oxides La_2O_3 and NiO. The mixed powders were first ball milled with isoamyl alcohol and air dried at 150 °C. The mixture was then dry ball milled to remove any inhomogeneity produced during the drying process. The loose powder was then placed in a platinum crucible and fired in flowing oxygen at 1120 °C for 12 h and slowly furnace cooled. The sample was again dry ball milled and fired in flowing nitrogen at 1035 °C for 4 h and furnace cooled. The resulting sample was a dark brown and/or black powder. One half of the 15-g sample was then annealed in flowing oxygen at 450 °C for 12 h and slowly cooled in oxygen to room temperature, resulting in a black powder. This pro-

cedure produced two 7.5-g samples with different oxygen contents: one sample annealed in oxygen ($\delta=0.18$), and one annealed in nitrogen ($\delta=0.07$). As will be described later, a third sample with $\delta=0.00$ was later prepared by partially reducing the oxygen-annealed sample in flowing hydrogen at 360 °C. The $\delta=0.00$ sample was a light yellowish-brown color.

THERMOGRAVIMETRIC ANALYSIS

The overall oxygen stoichiometries of the oxygen-annealed and nitrogen-annealed samples were determined by hydrogen reduction using a Perkin-Elmer TGA-7 system. The material was heated on a platinum pan in flowing hydrogen (0.1 L/min) to 700 °C at 2 °C/min. The weight-loss curves are shown in Fig. 1. Assuming that the level of impurity phases is small (as the neutron-diffraction data confirm) and that the phases resulting from the hydrogen reduction are Ni and La_2O_3, the overall oxygen stoichiometry of the oxygen-annealed sample is 4.18 ± 0.01, while that of the nitrogen-annealed sample is 4.07 ± 0.01.

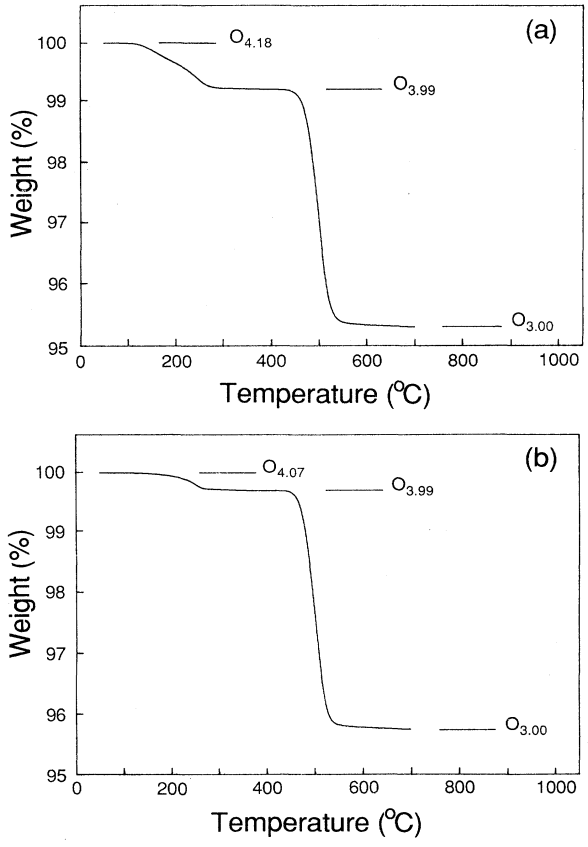

FIG. 1. Weight-loss curves for (a) oxygen-annealed and (b) nitrogen-annealed samples of $La_2NiO_{4+\delta}$ heated in flowing hydrogen. Assuming that the end products define an oxygen composition of 3.00, the beginning oxygen stoichiometry of the oxygen-annealed sample is 4.18 ± 0.01, while that of the nitrogen-annealed sample is 4.07 ± 0.01. Note that both weight-loss curves exhibit a broad plateau at an oxygen stoichiometry near 4.00 (the measured value is 3.99 ± 0.01) extending from 280 to 450 °C.

Both weight-loss curves show a well-defined, broad plateau at a measured oxygen stoichiometry of 3.99 ± 0.01 extending from 280 to 450 °C. The existence of this broad plateau in the oxygen-loss behavior suggested to us that (within the accuracy of our oxygen composition measurement) the stoichiometric compound, $La_2NiO_{4.00}$, is stable in hydrogen over this temperature range (at least for short times) and that a stoichiometric sample could be made by reducing an oxygen-rich sample in hydrogen at an appropriate temperature within this range. Thus, after completing the neutron-diffraction measurements on the oxygen-annealed ($\delta=0.18$) sample, we heated the sample to 350 °C in flowing 15 mol % H_2 in N_2 for 2 h, and then cooled rapidly to room temperature. This procedure produced a single-phase sample (assumed to be $\delta=0.00$) which was then also studied by neutron powder diffraction. Based on these hydrogen reduction measurements, we hereafter refer to the three samples studied by neutron powder diffraction as $La_2NiO_{4.00}$, $La_2NiO_{4.07}$, and $La_2NiO_{4.18}$.

NEUTRON POWDER DIFFRACTION

Neutron powder diffraction data were collected for these three samples at room temperature and at 10 K on the Special Environment Powder Diffractometer at Argonne's Intense Pulsed Neutron Source.[7] In addition, for the $La_2NiO_{4.07}$ sample, data were collected at intermediate temperatures of 100 and 200 K. For the low-temperature data collection the samples were contained in indium-sealed vanadium cans with 1 atm (at room temperature) of helium exchange gas. The high-resolution data from the backscattering detector banks ($2\theta=150°$) were used for Rietveld structure refinement.[8]

The structure of $La_2NiO_{4+\delta}$ has been reported to be tetragonal $I4/mmm$,[9–11] orthorhombic $Pban$,[12] or orthorhombic $Cmca$ ($Bmab$).[13] Rodriguez-Carvajal, however, argues that the report of $Pban$ symmetry is incorrect and resulted from interpreting a magnetic reflection as arising from nuclear scattering.[13] Additional confusion may arise from the fact that early authors did not fully appreciate that the system could exhibit such a wide range of oxygen stoichiometry resulting in substantial changes in the structural properties. For example, Odier *et al.*, observing this dependence on oxygen stoichiometry, reported that $La_2NiO_{4+\delta}$ prepared in oxygen atmospheres was tetragonal $I4/mmm$, while samples prepared in reducing conditions were orthorhombic.[14] Careful diffraction studies on single crystals by Rao *et al.*, however, show that for some oxygen stoichiometries samples which appear to index on a tetragonal cell are actually orthorhombic.[15] Rao *et al.* were able to index x-ray diffraction data for a single crystal of $La_2NiO_{4+\delta}$ ($\delta\approx0.2$) on the basis of a tetragonal cell ($a=3.88$ Å, $c=14.64$ Å); however, electron-diffraction data for the same crystal showed superlattice reflections corresponding to a $\sqrt{2}a\times\sqrt{2}a\times c$ orthorhombic superlattice. In the same study, a crystal with $\delta\approx0$ showed splittings of various reflections characteristic of a monoclinic unit cell. The same monoclinic cell for stoichiometric

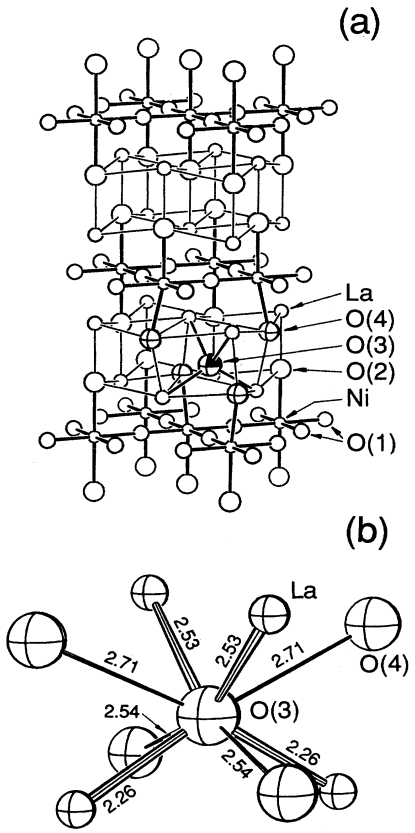

FIG. 2. Structure of the oxygen interstitial defect in $La_2NiO_{4+\delta}$. Atoms La, Ni, O(1), and O(2) occupy the normal lattice sites for the orthorhombic *Fmmm* La_2NiO_4 structure. O(3) is the interstitial oxygen defect, which is coordinated to four near-neighbor La atoms. Four near-neighbor O(2) atoms are displaced from their normal sites into new sites, O(4), which provide an acceptable O(3)-O(4) distance. At (a) one interstitial defect is shown in one unit cell (plus oxygen atoms coordinated to Ni) of the host structure. At (b) the local structure of the defect is shown, with interatomic distances labeled in Å.

La_2NiO_4 was later reported by Ram *et al.*,[16] although neither author has reported a structure refinement based on a monoclinic model.

Our raw neutron-diffraction data for $La_2NiO_{4.18}$ appeared to index on a tetragonal $I4/mmm$ cell. However, when refinements were attempted with this model, it was realized that systematic peak broadening consistent with a $\sqrt{2}a \times \sqrt{2}a \times c$ orthorhombic distortion was present. Thus, subsequent refinements were done in the corresponding orthorhombic space group *Fmmm*, resulting in significantly lower R values. The *Fmmm* space group was chosen by analogy to the La_2CuO_4 structure[1,17] and correctly indexes all of the peaks observed in the neutron powder diffraction data. In particular, no additional peaks which would suggest *Bmab* (the equivalent setting of *Cmca*) or lower orthorhombic symmetry were observed and we find no evidence for the closely related polar space group *Fmm*2 reported as the structure of Sm_2CoO_4.[18,19]

Initial refinements for the $La_2NiO_{4.18}$ sample at 295 and 10 K were done with atoms only in the normal lattice sites. When oxygen site occupancies were allowed to refine, a large vacancy concentration was observed at the apical oxygen site O(2) [see Fig. 2(a)]. This suggested that the excess oxygen was forming a defect which required the displacement of O(2) from its normal position. The most logical nearby interstitial site which could cause such a displacement is located near $(\frac{1}{4},\frac{1}{4},\frac{1}{4})$ in the orthorhombic *Fmmm* structure. Occupancy of this site by a peroxide ion has been proposed by Ganguly as a possible mechanism for the incorporation of excess oxygen.[20]

Based on this concept, refinement of a defect model was attempted. The oxygen interstitial defect, O(3), was placed at $(\frac{1}{4},\frac{1}{4},z;\ z\approx\frac{1}{4})$ and the apical oxygen was split into two sites, one at the normal position, O(2), $(0,0,z;\ z\approx 0.17)$ and the other at a displaced site, O(4), $(x,y,z;\ x\approx y\approx -0.06,\ z\approx 0.17)$ as shown in Fig. 2. The initial values for x(O(4)) and y(O(4)) were chosen to provide a sensible distance between O(3) and O(4) with a displacement directly away from O(3). Initial refinements where the O(3) and O(4) atom positions were constrained showed positive occupancy at both sites. Final refinements were then done with variable atom positions and site occupancies for both O(3) and O(4) and with no overall constraint on oxygen site occupancies. Although the values of other parameters, including the site occupancies, did not change, a significant improvement in R values was achieved by assigning an anisotropic temperature factor to the basal-plane oxygen O(1). As was also observed in $La_2CuO_{4+\delta}$,[1] O(1) exhibits large (thermal or static) displacements perpendicular to the basal plane. It was found to be necessary to constrain the temperature factors of the defect oxygen atoms; $B(O(3))=1$ Å^2 and $B(O(4))=B(O(2))$. The final refinement included 413 *Fmmm* Bragg reflections extending over d spacings from 0.52 to 3.18 Å. The results of this refinement are given in Table I and a plot of part of the refinement profile is shown in Fig. 3.

The data for $La_2NiO_{4.18}$ at 10 K were also refined in the *Fmmm* space group. Refined parameters are given in Table I. As expected, the same defect is present. The small variations in site occupancies probably result from the fact that [except for O(1)] the temperature factors are not refined anisotropically. Thus, any anisotropic behavior, which would be expected to vary with temperature, may appear as a correlated error in the site occupancies. This effect would be especially significant for the apical oxygen O(2), which is known to exhibit an anisotropic Debye-Waller factor with the largest displacements perpendicular to the c axis.[21,22]

The internal consistency and agreement of the defect concentration with that measured by hydrogen reduction are remarkable. Such a refinement in which the site occupancies are not constrained provides a strict test of the validity of the defect model. Occupancy of one O(3) defect position would be expected to displace four neighboring O(2) atoms into the O(4) site. Thus, the model is judged to be valid if $n(O(2))+n(O(4))\approx 2$ and $n(O(4))\approx 4n(O(3))$. The refined defect occupancy at O(3) is 0.16(2) at 295 K and 0.18(1) at 10 K in excellent agreement with the hydrogen reduction value, 0.18(1). Additionally the occupancies at O(3) and O(4) are in a

TABLE I. Refined structural parameters for $La_2NiO_{4+\delta}$, $\delta=0.00$ and 0.18. The data are refined in orthorhombic space groups *Bmab* and *Fmmm*, respectively. Numbers in parentheses are standard deviations of the last significant digit. Where no standard deviation is given, the value was not refined. R_{wp} and R_{exp} are the weighted profile and expected R values, respectively.

		$\delta=0$	$\delta=0.18$	
	T (K)	295	295	10
	Space group	*Bmab*	*Fmmm*	*Fmmm*
a	(Å)	5.4656(1)	5.4614(2)	5.4469(1)
b	(Å)	5.5327(1)	5.4723(2)	5.4569(1)
c	(Å)	12.5547(3)	12.7138(2)	12.6637(2)
V	(Å^3)	379.66(2)	379.96(3)	376.40(2)
La	*x*	0	0	0
	y	−0.0099(5)	0	0
	z	0.3636(1)	0.3600(1)	0.3601(1)
	B (Å^2)	0.14(3)	0.44(3)	0.25(2)
	n	2	2	2
Ni	$x=y=z$	0	0	0
	B (Å^2)	0.19(4)	0.30(3)	0.19(2)
	n	1	1	1
O(1)	$x=y$	$\frac{1}{4}$	$\frac{1}{4}$	$\frac{1}{4}$
	z	−0.0087(5)	0	0
	U_{11} (Å^2)	0.002(1)	0.000(2)	0.001(1)
	U_{22} (Å^2)	0.004(1)	0.006(2)	0.004(1)
	U_{33} (Å^2)	0.018(2)	0.030(1)	0.025(1)
	U_{12} (Å^2)	−0.004(1)	−0.002(1)	−0.000(1)
	$U_{13}=U_{23}$ (Å^2)	0	0	0
	n	2	2	2
O(2)	*x*	0	0	0
	y	0.0364(7)	0	0
	z	0.1793(3)	0.1733(5)	0.1731(3)
	B (Å^2)	0.99(8)	0.7(1)	0.45(6)
	n	2.04(4)	1.14(4)	1.22(2)
O(3)	$x=y$	$\frac{1}{4}$	$\frac{1}{4}$	$\frac{1}{4}$
	z	0.23	0.232(4)	0.235(3)
	B (Å^2)	1	1	1
	n	0.01(2)	0.16(2)	0.18(1)
O(4)	*x*	−0.064	−0.060(3)	−0.065(2)
	y	−0.064	−0.069(3)	−0.069(2)
	z	0.173	0.172(1)	0.1717(7)
	B (Å^2)	$=B$(O(2))	$=B$(O(2))	$=B$(O(2))
	n	0.02(4)	0.84(5)	0.76(2)
R_{wp}	(%)	7.48	7.95	6.15
R_{exp}	(%)	5.26	4.89	2.61
With constraints n(O(4))=4n(O(3)) and $n(2)+n(4)=2$				
O(3)	*n*		0.200(7)	0.189(4)
R_{wp}	(%)		7.96	6.15
With no defect				
R_{wp}	(%)	7.51	8.68	7.34

nearly perfect 1:4 ratio, especially for the 10-K data, and n(O(2))+n(O(4)) is equal to 2 within the standard deviations. For comparison, the refined defect concentrations for a model in which the site occupancies are constrained as described above is also given in Table I.

The 295-K data for $La_2NiO_{4.00}$ were refined in the orthorhombic *Bmab* space group analogous to La_2CuO_4.[17] In this case, the orthorhombic stain is much larger and is easily visible in the raw data. Additionally, the Bragg peaks arising from the lower, *Bmab*, symmetry are readily observed. (The *Bmab* setting was chosen rather than the standard *Cmca* setting in order to allow a direct comparison with the *Fmmm* results.) The *Bmab* refinement included 739 Bragg reflections over a *d* spacing range of 0.52–3.18 Å. The refined parameters are included in Table I and a plot of part of the refinement profile is shown in Fig. 4. As shown in Table I, inclusion of the same interstitial oxygen defect in the refinement led to

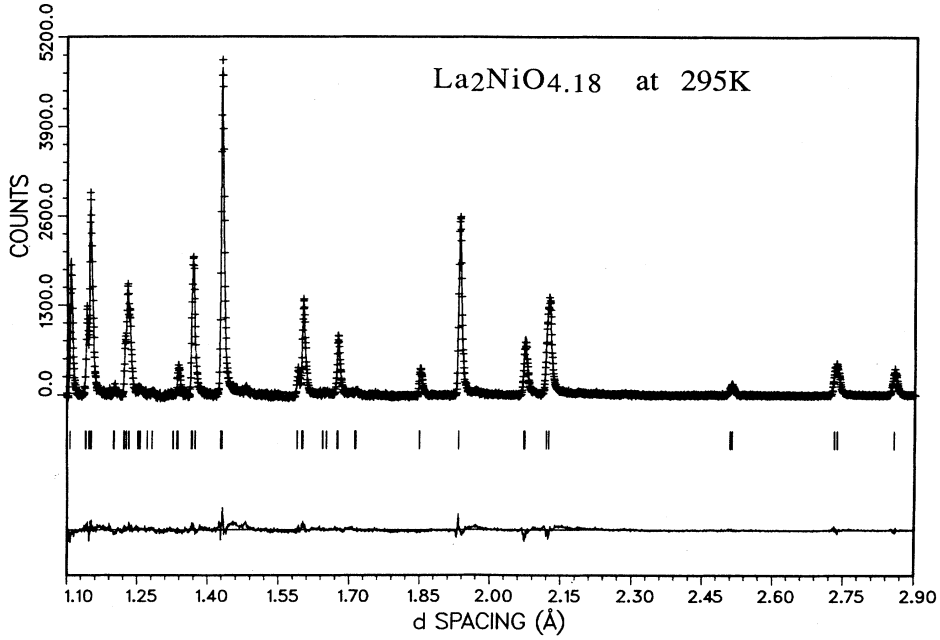

FIG. 3. Portion of the Rietveld refinement profile for orthorhombic (*Fmmm*) $La_2NiO_{4.18}$ at 295 K. Plus marks (+) are the raw data. The solid line is the calculated profile. Tick marks below the profile mark the positions of allowed reflections. A difference curve (observed minus calculated) is plotted by the bottom. Background has been fit as part of the refinement but subtracted prior to plotting.

near-zero occupancies for both O(3) and O(4) and essentially full occupancy for O(2). It should be noted that because of the differences in symmetry, the description of the defect is not strictly the same in the *Bmab* and *Fmmm* space groups. However, we refined the $La_2NiO_{4.18}$ data in *Bmab* symmetry and obtained the same defect concentrations as for *Fmmm*, giving us confidence that inclusion of the same defect model in *Bmab* symmetry was a valid test of the existence of the defect. Thus, the $La_2NiO_{4.00}$ refinement provides an additional satisfying confirmation of the validity of the defect model.

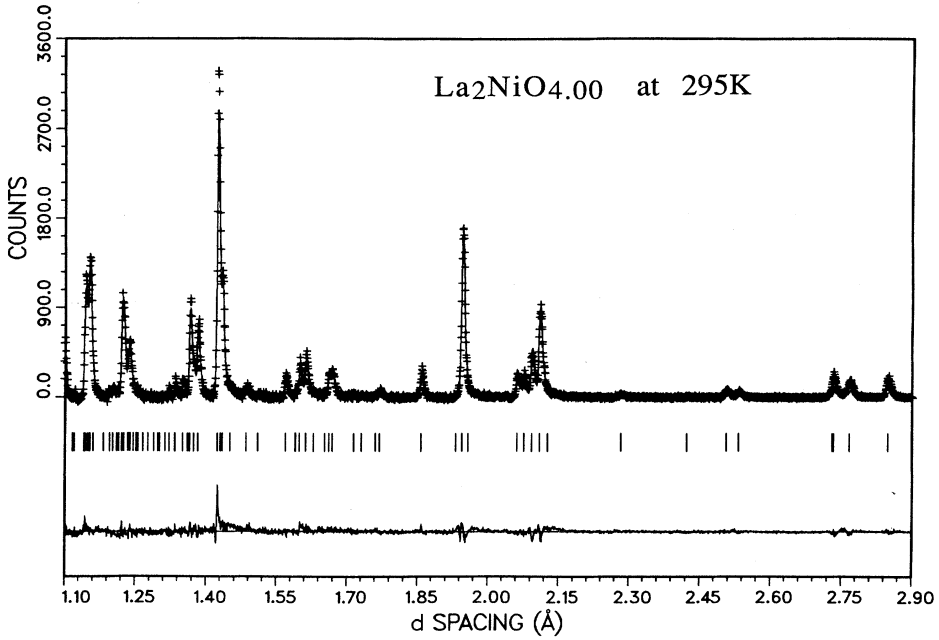

FIG. 4. Portion of the Rietveld refinement profile for orthorhombic (*Bmab*) $La_2NiO_{4.00}$ at 295 K. Format is the same as for Fig. 3.

TABLE II. Refined structural parameters for the two phases of the mixed-phase sample with bulk composition $La_2NiO_{4.07}$. The two phases are in the orthorhombic *Bmab* and *Fmmm* space groups, as in Table I. The refinements are stabilized by constraining $B(A)_{Bmab}=B(A)_{Fmmm}$ for A=La,Ni,O(1),O(2), and by constraining the oxygen site occupancies to match our physical model of the defect, i.e., $n(O(4))=4n(O(3))$ and $n(O(2))+n(O(4))=2$.

	T (K)	295		200	
	R_{wp}/R_{expt}	0.0630/0.0353		0.0707/0.0446	
	Phase	*Bmab*	*Fmmm*	*Bmab*	*Fmmm*
a	(Å)	5.4714(3)	5.4863(3)	5.4590(2)	5.4844(3)
b	(Å)	5.4799(3)	5.4953(2)	5.4879(2)	5.4973(3)
c	(Å)	12.6228(5)	12.5768(4)	12.6098(5)	12.5548(5)
V	(Å^3)	378.47(4)	379.18(4)	377.77(4)	378.51(4)
La	x	0	0	0	0
	y	−0.0076(7)	0	−0.0092(8)	0
	z	0.3635(2)	0.3619(2)	0.3631(2)	0.3620(3)
	B (Å^2)	0.43(2)	=B(*Bmab*)	0.21(2)	=B(*Bmab*)
	n	2	2	2	2
Ni	$x=y=z$	0	0	0	0
	B (Å^2)	0.49(2)	=B(*Bmab*)	0.28(3)	=B(*Bmab*)
	n	1	1	1	1
O(1)	$x=y$	$\frac{1}{4}$	$\frac{1}{4}$	$\frac{1}{4}$	$\frac{1}{4}$
	z	−0.0010(4)	0	−0.0095(5)	0
	B (Å^2)	0.65(3)	=B(*Bmab*)	0.45(4)	=B(*Bmab*)
	n	2	2	2	2
O(2)	x	0	0	0	0
	y	0.031(1)	0	0.032(1)	0
	z	0.1778(5)	0.1782(6)	0.1786(6)	0.1778(7)
	B (Å^2)	1.03(5)	=B(*Bmab*)	0.82(6)	=B(*Bmab*)
	n	=2−n(O(4))	=2−n(O(4))	=2−n(O(4))	=2−n(O(4))
O(3)	$x=y$	$\frac{1}{4}$	$\frac{1}{4}$	$\frac{1}{4}$	$\frac{1}{4}$
	z	0.235	0.235	0.235	0.235
	B (Å^2)	1	1	1	1
	n	0.0029(1)	0.110(7)	0.0029(1)	0.108(9)
O(4)	x	−0.064	−0.064	−0.064	−0.064
	y	−0.064	−0.064	−0.064	−0.064
	z	0.177	0.176	0.177	0.176
	B (Å^2)	=B(O(2))	=B(O(2))	=B(O(2))	=B(O(2))
	n	=4n(O(3))	=4n(O(3))	=4n(O(3))	=4n(O(3))
Scale	only factor	0.79(2)	0.73(2)	0.40(1)	0.36(1)
Faction	(%)	52(2)	48(2)	53(2)	47(2)

The 12-K data for $La_2NiO_{4.00}$ could not be refined in a *Bmab* model. From the raw data, it is clear that the system is either partially or fully transformed to a different structure. Rodriguez-Carvajal *et al.* observed an unusual phase transition in La_2NiO_4 near 70 K and interpreted their data in the same *Cmca* (*Bmab*) space group, but with a reduced orthorhombic strain and a discontinuous change in the internal atom displacements.[13] Our data, which are taken at higher resolution and over a much broader range of d spacings, confirm the existence of this phase transition but disagree markedly with their conclusions. Based on the raw diffraction data, we suspect that $La_2NiO_{4.00}$ exhibits the same complex phase transition behavior observed in $La_{2-x}Ba_xCuO_4$ at low temperature.[23,24] Originally, that system was also reported to undergo an unusual transition involving a sudden reduction in the orthorhombic strain.[23] However, recent extensive work reported by Axe *et al.* shows that the actual transition involves the sequential softening of lattice phonons resulting in transitions from $I4/mmm$ to *Cmca* and then (near 70 K) to $P4_2/ncm$, and that interpretation of the low-temperature data is, unfortunately, confused by the fact that the latter transition is often sluggish, resulting in a partial transition.[25] Such a conclusion is consistent with our raw data, but since this point is not relevant to the subject of this paper, we have not pursued it further.

Our data for $La_2NiO_{4.07}$ show clear two-phase behavior at all temperatures. This observation suggests a phase separation similar to that observed in $La_2CuO_{4+\delta}$.[1] The separations between Bragg peaks from the two phases grow with decreasing temperature such that below 200 K, many peaks from the two phases are clearly resolved and it was straightforward to conclude that the raw data could be indexed on the basis of two orthorhombic phases, one of which exhibited a larger orthorhombic

TABLE II. (*Continued*).

T (K)		100		10	
R_{wp}/R_{expt}		0.0713/0.0449		0.0651/0.0319	
Phase		*Bmab*	*Fmmm*	*Bmab*	*Fmmm*
a	(Å)	5.4535(2)	5.4839(3)	5.4516(2)	5.4839(3)
b	(Å)	5.4885(2)	5.4978(2)	5.4892(2)	5.4981(2)
c	(Å)	12.5927(5)	12.5326(4)	12.5863(5)	12.5553(5)
V	(Å^3)	376.92(2)	377.85(2)	376.64(2)	378.56(2)
La	x	0	0	0	0
	y	−0.0105(8)	0	−0.0110(6)	0
	z	0.3628(3)	0.3624(3)	0.3630(2)	0.3623(2)
	B (Å^2)	0.06(2)	$=B(Bmab)$	0.01(2)	$=B(Bmab)$
	n	2	2	2	2
Ni	$x=y=z$	0	0	0	0
	B (Å^2)	0.21(3)	$=B(Bmab)$	0.14(2)	$=B(Bmab)$
	n	1	1	1	1
O(1)	$x=y$	$\frac{1}{4}$	$\frac{1}{4}$	$\frac{1}{4}$	$\frac{1}{4}$
	z	−0.0102(4)	0	−0.0105(3)	0
	B (Å^2)	0.37(3)	$=B(Bmab)$	0.34(3)	$=B(Bmab)$
	n	2	2	2	2
O(2)	x	0	0	0	0
	y	0.031(1)	0	0.034(1)	0
	z	0.1790(5)	0.1774(7)	0.1735(3)	0.1767(6)
	B (Å^2)	0.72(5)	$=B(Bmab)$	0.53(5)	$=B(Bmab)$
	n	$=2-n(O(4))$	$=2-n(O(4))$	$=2-n(O(4))$	$=2-n(O(4))$
O(3)	$x=y$	$\frac{1}{4}$	$\frac{1}{4}$	$\frac{1}{4}$	$\frac{1}{4}$
	z	0.235	0.235	0.235	0.235
	B (Å^2)	1	1	1	1
	n	0.0028(1)	0.148(4)	0.0028(1)	0.134(8)
O(4)	x	−0.064	−0.064	−0.064	−0.064
	y	−0.064	−0.064	−0.064	−0.064
	z	0.177	0.176	0.177	0.176
	B (Å^2)	$=B(O(2))$	$=B(O(2))$	$=B(O(2))$	$=B(O(2))$
	n	$=4n(O(3))$	$=4n(O(3))$	$=4n(O(3))$	$=4n(O(3))$
Scale	only factor	0.401(8)	0.344(8)	0.80(2)	0.68(1)
Faction	(%)	54(2)	46(2)	54(2)	46(2)

splitting than the other. Refinements were, thus, attempted with a two-phase, *Bmab* plus *Fmmm*, model using the $La_2NiO_{4.00}$ and $La_2NiO_{4.18}$ structural parameters (Table I) as starting values. Unconstrained two-phase refinements readily yielded accurate fits to the data at all temperatures. However, the refined values for the oxygen site occupancies were not stable enough to provide meaningful physical conclusions. We conclude that this instability results from a high correlation between corresponding parameters in the two phases [e.g., correlations between B(La) for the *Bmab* phase and B(La) for the *Fmmm* phase]. The situation is, undoubtedly, exacerbated in the present case by the fact that the two phases are nearly identical structures in which many of the corresponding peaks are overlapped.

Stable refinements of the two-phase data were achieved by applying a small number of constraints. The temperature factors of the *Bmab* phase were constrained to be equal to the temperature factors of the *Fmmm* phase [e.g., $B(\mathrm{La})_{Bmab}=B(\mathrm{La})_{Fmmm}$, etc.]. Additionally, for each phase the site occupancies defining the defect were constrained to obey the physically expected behavior, i.e., $n(O(4))=4n(O(3))$ and $n(O(2))+n(O(4))=2$. Using these constraints, the refinements quickly converged for all temperatures. The refined structural parameters are presented in Table II and part of the Rietveld refinement profile (for the data at 200 K, where the peak splittings can be more clearly seen) is shown in Fig. 5.

When combined with the bulk oxygen content measured by hydrogen reduction, the defect site occupancies from the two-phase refinements for the $La_2NiO_{4.07}$ sample allow the miscibility gap to be approximately located in the oxygen-concentration phase diagram for temperatures below room temperature. The best estimates are made by averaging the values for the four sample temperatures. In doing so, we assume that the phase separation is essentially complete at 300 K, and that our data are not of sufficient accuracy to detect small changes in composition which could result from oxygen diffusion at lower temperatures. For the oxygen-rich *Fmmm* phase,

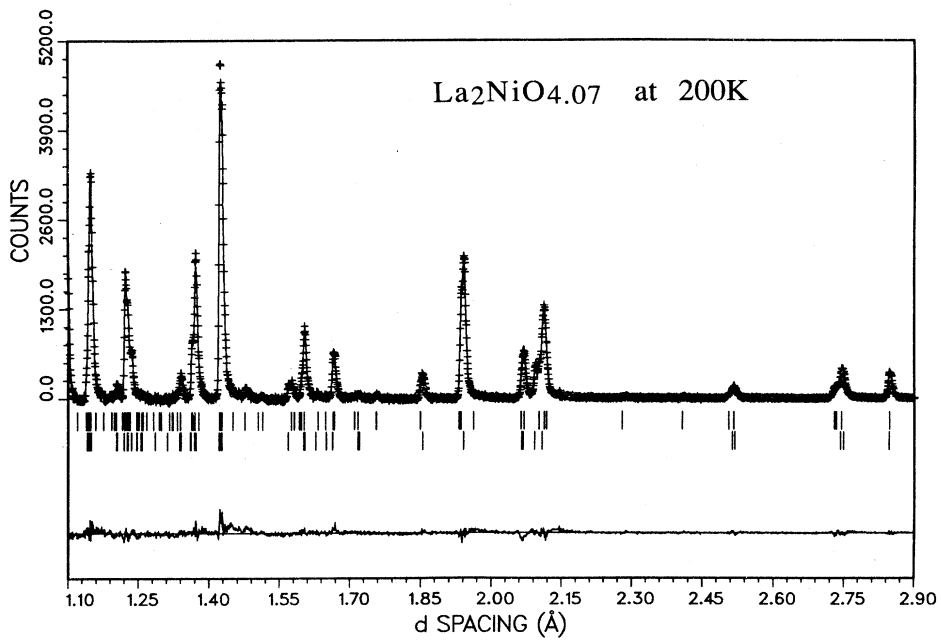

FIG. 5. Portion of the Rietveld refinement profile for $La_2NiO_{4.07}$ at 200 K refined with a two-phase model based on *Bmab* and *Fmmm* orthorhombic phases. Format is the same as for Fig. 3 except that the top row of tick marks is for one phase and the bottom row is for the other.

the oxygen stoichiometry estimated from the Rietveld refinements is $\delta=0.12-0.13$. For the *Bmab* phase, the defect concentration (based on the same model) consistently refines to zero. We will later argue that this seemingly inconsistent result occurs because the configuration of the excess oxygen defect is not the same in the *Bmab* and *Fmmm* phases and, thus, the concentration of this particular interstitial defect is, indeed, zero in the *Bmab* phase.

Other structural parameters, however, clearly show that the *Bmab* phase does have a finite solubility for excess oxygen. For example, at 295 K the *Bmab* phase exhibits a much smaller orthorhombic strain than $La_2NiO_{4.00}$. This result can be compared with the observation that the orthorhombic strain is also reduced very quickly by doping La_2CuO_4 with Sr on the La site.[26] In that case $La_{2-x}Sr_xCuO_4$ transforms from orthorhombic to tetragonal near $x=0.05$ at 295 K and near $x=0.2$ at 10 K.

From our data, it is not possible to directly determine the maximum solubility for excess oxygen in the *Bmab* phase. However, an approximate value can be estimated from the refined defect concentration in the *Fmmm* phase ($\delta=0.125$ averaged over four temperatures) and the bulk oxygen concentration measured by hydrogen reduction ($\delta=0.07$). The relative abundance of the two phases in the $La_2NiO_{4.07}$ sample is obtained from the refined scale factors (Table II). Based on this approximation, the maximum solubility for excess oxygen in the *Bmab* phase is $\delta=0.02$. Unfortunately, because of uncertainties in both the hydrogen reduction and structural results, the error bars on this value are asymmetric and could be large—perhaps $-0.01/+0.03$. Nevertheless, the general features of the phase diagram are not in question.

An approximate phase diagram, based on our limited data is shown in Fig. 6. The transition from orthorhombic (O^I) to tetragonal (T) at $\delta=0$ and 700 K is based on the work of Rodriguez-Carvajal *et al.*[13] The temperature at which the O^I-T transition intersects the miscibility gap (near $\delta=0.02$) is estimated from the temperature dependence of the orthorhombic strain (b-a) for the *Bmab* phase of the two-phase sample (see Fig. 7). At least three phases are present: the orthorhombic (*Bmab*) O^I phase, which exhibits a solubility for excess oxygen up to about 0.02 at room temperature, the tetragonal (*I4/mmm*) T phase, to which the O^I phase transforms at high temperature, and the orthorhombic (*Fmmm*) O^{II} phase, which exists for $\delta>0.13$ at room temperature and which contains the specific oxygen interstitial defect presented in

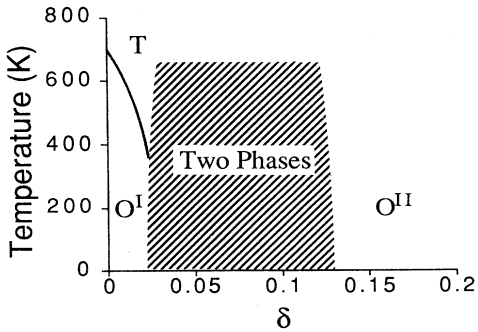

FIG. 6. Approximate structural phase diagram for $La_2NiO_{4+\delta}$. O^I and O^{II} are orthorhombic *Bmab* and *Fmmm* phases, respectively, with differing solubilities for excess lattice oxygen and T is a tetragonal *I4/mmm* phase. The shaded region is the approximate location of the miscibility gap as determined from a two-phase $\delta=0.07$ sample.

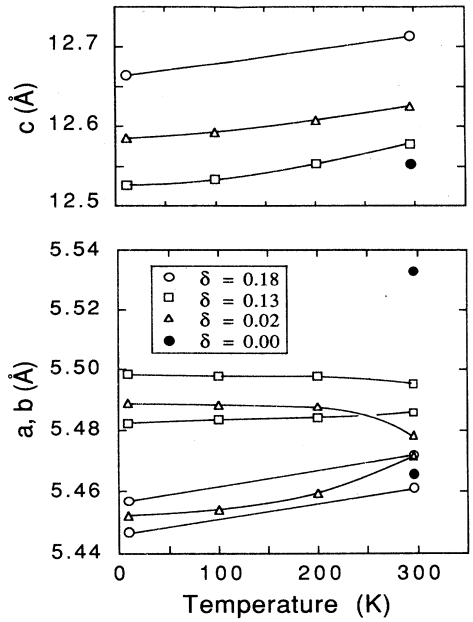

FIG. 7. Lattice parameters for four compositions of $La_2NiO_{4+\delta}$ ($\delta=0.00$, 0.02, 0.13, and 0.18) as a function of temperature. The data for $\delta=0.02$ and 0.13 are obtained from Rietveld refinements for a two-phase sample of bulk composition $La_2NiO_{4.07}$. In the case of $\delta=0.00$, no 10-K data are available because of a transition to another phase (see the text).

this paper. Since no data were taken above 300 K, we cannot comment on the details of the phase diagram at higher temperatures. In particular, we have not determined the temperature at which phase separation begins, the location of the phase line between the O^{II} and T phases, or the nature of the O^{II}-T transition.

The measured lattice constants for the four compositions of $La_2NiO_{4+\delta}$, $\delta=0.00$, 0.02, 0.13, and 0.18, are plotted as a function of temperature in Fig. 7. The orthorhombic strain for $La_2NiO_{4.02}$ is much smaller than for $La_2NiO_{4.00}$ at room temperature and increases significantly with decreasing temperature. Thus, in the O^I phase the strain exhibits the expected temperature and composition dependence for an order parameter near a soft phonon mode transition.[27,28] However, for both $La_2NiO_{4.13}$ and $La_2NiO_{4.18}$ the orthorhombic strain, even though it is small, shows no appreciable temperature or composition dependence. Thus, if this orthorhombic strain is the result of a softened phonon mode, the O^{II}-T transition must be at much higher temperatures. A possible conclusion is that the orthorhombic distortion for $\delta=0.13$ and 0.18 can most logically be viewed as resulting from the incorporation of the oxygen interstitial defect and not from a conventional soft-phonon-mode transition, as is the case in the *Bmab* phase at lower values of δ.

The topology of this phase diagram and the behavior of the structural parameters supports our hypothesis that the oxygen defect structures in the *Bmab* and *Fmmm* phases must differ in some subtle way. Indeed, without a subtle structural difference the miscibility gap would not exist. Unfortunately, the solubility for excess oxygen is so small in the O^I phase that we have little chance of directly determining its defect structure from diffraction data, even if we had a single-phase ($\delta\approx0.02$) sample. Examination of the lattice constants and unit cell volume as a function of δ, as plotted in Fig. 8, does, however, provide evidence that the excess oxygen is incorporated differently in the two phases. The most striking evidence is provided by the behavior of the cell volume, which contracts in the *Bmab* phase and expands in the *Fmmm* phase with increasing δ. Such behavior implies that the oxygen defect also produces different electronic effects in the *Bmab* and *Fmmm* phases. The c axis expands with increasing δ for $0<\delta<0.02$, drops to a lower value upon crossing the miscibility gap, and then expands again for $0.13<\delta<0.18$. At the same time, the average basal-plane lattice parameter, $(a+b)/2$, contracts with increasing δ in both phases, with an offset upon crossing the miscibility gap. Thus, as expected, the distortion in lattice parameters caused by the incorporation of excess oxygen in the O^I (*Bmab*) phase is relaxed upon crossing the miscibility gap, i.e., by incorporating the excess oxygen into a defect with a different structure, but then increases again with increasing δ in the O^{II} (*Fmmm*) phase.

THE OXYGEN INTERSTITIAL DEFECT

The local configuration of the oxygen interstitial defect for $0.13<\delta<0.18$ is illustrated in Fig. 2. Since the refinement provides only a spatial average of the actual structure, the refinement results must be combined with chemical intuition to understand the local structure of

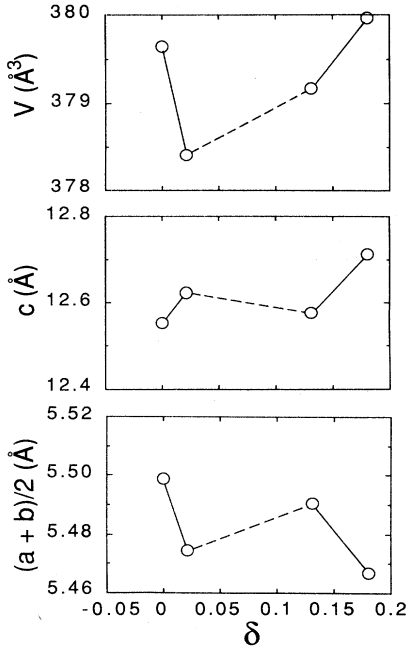

FIG. 8. Lattice parameters, $(a+b)/2$ and c, and unit cell volume, V, for $La_2NiO_{4+\delta}$ vs δ at 295 K. The values of δ for $\delta=0.02$ and 0.13 are approximated from the combined results of Rietveld refinement and hydrogen reduction of a two-phase sample (see the text). For $\delta=0.00$ and 0.18, the values are those determined by hydrogen reduction of single-phase samples.

the defect. In a single interstitial location, *Fmmm* symmetry defines one O(3) atom at $(\frac{1}{4},\frac{1}{4},z)$ and a symmetry-equivalent atom at $(\frac{1}{4},\frac{1}{4},\frac{1}{2}-z)$ $(z\approx 0.23)$. Because of their close proximity, only one of these two sites can be occupied. Average *Fmmm* symmetry is achieved if the choice is random. For the purposes of our discussion we choose to place the defect at $(\frac{1}{4},\frac{1}{4},0.23)$. Obviously, we assume that the four O(2) atoms which are displaced into O(4) sites are those which neighbor the defect at O(3). Furthermore, even though the *Fmmm* symmetry defines four O(4) positions near each O(2) site, we assume that the O(4) site which is actually occupied in a given cell is the one which achieves the longest O(3)-O(4) distance. These assumptions have been used to define the local defect structure shown in Fig. 2 and to calculate the interatomic distances in Table III.

As a test of the validity of the proposed defect, it is useful to look at interatomic distances in the structure. The relevant distances are given in Table III, and illustrated in Fig. 2(b). Since the defect is located at $z=0.23$, and not at $z=\frac{1}{4}$, the local configuration has two short and two long La-O(3) bonds and, likewise, two short and two long O(3)-O(4) distances. We realize at this point, that the assignment of equal displacements for the O(4) atoms above and below the O(3) defect is only an approximation to the local defect structure. Moreover, small local displacements of La are probably also present. These small differences are, perhaps, what gives rise to the small orthorhombic distortion of an otherwise tetragonal structure. However, the present defect model appears to be adequate to characterize the basic features of the defect structure and is probably the best approximation that can be achieved within the *Fmmm* symmetry of the host structure.

TABLE III. Interatomic distances in $La_2NiO_{4+\delta}$ as determined from Rietveld refinement of neutron powder diffraction data. Numbers in parentheses are standard deviations of the last significant digit. In the case of the distances involving the interstitial defect at O(3), only the physically reasonable distances are given (see the text).

	Interatomic distance (Å)		
	$\delta=0$	$\delta=0.18$	
T (K)	295	295	10
Host structure			
Ni-O(1)	1.9486(2)	1.9328(1)	1.9275(1)
Ni-O(2)	2.261(4)	2.202(6)	2.192(4)
La-O(1)	2.538(3)	2.628(1)	2.6180(8)
	2.654(3)		
La-O(2)	2.324(4)	2.375(6)	2.369(4)
	2.7891(8)	2.769(1)	2.7606(6)
	2.569(4)	2.7631(6)	2.7556(6)
O(1)-O(1)	2.7328(1)	2.7307(1)	2.7235(1)
	2.7785(7)	2.7361(1)	2.7284(1)
O(2)-O(2)	3.283(4)	3.362(7)	3.353(4)
	3.287(4)	3.357(7)	3.349(4)
	3.612(5)		
O(1)-O(2)	2.981(4)	2.930(5)	2.919(3)
Defect structure			
Ni-O(4)		2.25(1)	2.24(1)
La-O(3)		2.53(3)	2.49(2)
		2.26(2)	2.28(2)
La-O(4)		2.43(1)	2.44(1)
		2.42(2)	2.41(1)
		2.47(2)	2.43(1)
O(2)-O(3)[a]		2.07(2)	2.08(1)
		2.28(2)	2.25(2)
O(3)-O(4)[b]		2.54(2)	2.57(2)
		2.71(3)	2.71(2)

[a]This distance is not physically meaningful since the presence of the defect at O(3) displaces O(2) from its ideal positions (see the text).

[b]In the case of O(3)-O(4), only the long, physically meaningful, distances are listed (see the text).

The shortest La-O(3) distance, 2.26 Å is somewhat shorter than the shortest La-O distance in the host structure (2.32 Å), but is not unreasonable based on expected ionic radii, realizing that the effective radius of La varies widely depending on coordination. The small discrepancy could result from small local La displacements around the O(3) defect which we have not included in our refinement model. Likewise, the shortest O(3)-O(4) distance, 2.54 Å, is not unacceptable, especially in light of the fact that we have approximated the O(4) displacements by assigning the same displacements to all O(4) atoms. The interatomic distances of the host lattice, e.g., La-O(1), La-O(2), Ni-O(1), Ni-O(2), are only marginally perturbed by the incorporation of the defect. It is interesting to note, however, that the Ni—O bonds are systematically shortened, consistent with the concept of charge transfer from the oxygen interstitial defect to the Ni-O layer.

Individual Ni—O bond lengths probably provide the most sensitive probe of the electronic effects of the oxygen defects in the *Bmab* and *Fmmm* phases. Based on observations in the $YBa_2Cu_3O_{7-x}$ structure, we would expect the bridging Ni—O(2) bond, which connects the conducting two-dimensional layer to the double LaO layer, to be the most sensitive to charge transfer.[29] The Ni—O bond lengths versus δ are shown in Fig. 9. As expected, the largest variations are observed for Ni-O(2). Interestingly, the behavior is quite different for the *Bmab* and *Fmmm* phases, in agreement with our conclusion that different oxygen defects are formed. In the *Fmmm* phase, the Ni—O(2) bond shortens significantly with increasing δ, consistent with the expected charge transfer from an O^{2-} interstitial defect. In the *Bmab* phase, however, negligibly small bond length changes are observed, suggesting that no charge is transferred. One possible explanation for this behavior is that a charge-neutral defect is formed in the *Bmab* phase.

Several authors have proposed the existence of a peroxide or superoxide defect as a possible mechanism for incorporating excess oxygen into $La_2NiO_{4+\delta}$ and $La_2CuO_{4+\delta}$.[3,4,20,30] These proposals have been based on experimental evidence such as comparisons of thermogravimetric analysis and iodometric titration, magnetization data, and x-ray photoelectron spectroscopy. Zhou *et al.* have recently challenged these ideas by showing that the experimental evidence for a superoxide species may be associated with "superficial oxygen" (e.g., a surface species)

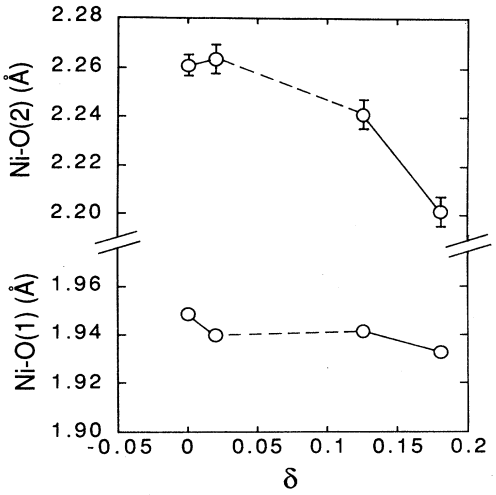

FIG. 9. Ni—O bond lengths vs δ at 295 K as determined by Rietveld refinement of neutron powder diffraction data.

rather than bulk excess oxygen in the $La_2CuO_{4+\delta}$ compound.[31] Our results offer another possible explanation for the persistent indications of a peroxide or superoxide species. The interstitial site near $(\frac{1}{4},\frac{1}{4},z;\ z\approx\frac{1}{4})$ is apparently not large enough to accommodate a superoxide ion or peroxide ion oriented along the z direction. To do so would require both of the symmetry-equivalent $(\frac{1}{4},\frac{1}{4},z)$ and $(\frac{1}{4},\frac{1}{4},\frac{1}{2}-z)$ sites to be simultaneously occupied with $z<0.2$. Our data clearly show that for the *Fmmm* phase with $0.13<\delta<0.18$ the defect at this site is a single interstitial oxygen atom. However, we are not able to determine the structure of the oxygen defect in the *Bmab* phase for $0<\delta<0.02$. The variation of unit cell volume with δ (Fig. 8) suggests that a defect with a substantially different structure is formed. Thus, the existence of a superoxide or peroxide defect in the *Bmab* phase is not excluded by our data. Moreover, if such a defect does exist, we are not able to specify its location in the structure. While the $(\frac{1}{4},\frac{1}{4},\frac{1}{4})$ site appears to be ruled out, it may be possible for a superoxide or peroxide ion to substitute at one of the normal lattice oxygen sites, O(1) or O(2), as proposed by Buttrey *et al.*[4] For example, the displacement of the O(2) oxygen atom into the O(4) site which we observe (0.5 Å) is nearly large enough to allow the accommodation of such a defect substitutionally at the O(2) site. We also note that a peroxide or superoxide ion substitutional defect would produce a very different electronic effect, in agreement with our Ni—O bond-length data (Fig. 9). Such a proposal is, of course, entirely speculative and must await experimental verification when suitable structural data are available for the oxygen defect in the *Bmab* phase.

SUMMARY AND CONCLUSIONS

In summary, we have synthesized three samples of $La_2NiO_{4+\delta}$ with widely different oxygen contents ($\delta=0.00$, 0.07, and 0.18) and have used these samples to study the structural mechanism by which excess oxygen is incorporated into the structure and the general features of the oxygen-concentration phase diagram. For the $La_2NiO_{4.18}$ sample, which is single phase, we have been able to determine the structure of an interstitial oxygen defect which is located at the $(\frac{1}{4},\frac{1}{4},z;\ z\approx0.23)$ site in the orthorhombic *Fmmm* lattice. This defect allows the interstitial oxygen atom to be favorably coordinated to four neighboring La atoms, but requires four neighboring oxygen atoms to be displaced ~0.5 Å from their normal lattice sites.

The $La_2NiO_{4.07}$ sample is separated into an oxygen-rich orthorhombic *Fmmm* phase and a nearly stoichiometric orthorhombic *Bmab* phase. Changes in the lattice constants for the *Bmab* phase, as compared to those observed for a $La_2NiO_{4.00}$ sample, show conclusively, however, that the solubility for excess oxygen in the *Bmab* phase is not zero. Our best estimates for the compositions of the two phases near room temperature, based on Rietveld refinements of neutron powder diffraction data and hydrogen reduction, define a phase diagram (Fig. 6) where the *Bmab* phase exists for $0<\delta<0.02$ and the *Fmmm* phase exists for $0.13<\delta<0.18$. Although the quantitative assignment of stability ranges for these two phases is subject to a number of errors, the general topology of the phase diagram is not in question. An additional important observation from this work is that the excess oxygen which can be incorporated into the *Bmab* phase ($0<\delta<0.02$) probably involves a different defect structure. Our observation of a very different dependence of the unit cell volume on δ for the *Bmab* and *Fmmm* phases supports this conclusion. A solution of the oxygen defect structure for the *Bmab* phase must await the synthesis of single-phase *Bmab* samples with excess oxygen and may, in fact, be possible only by single-crystal techniques, owing to the small solubility.

These results for $La_2NiO_{4+\delta}$ are remarkably similar to those previously reported for $La_2CuO_{4+\delta}$.[1] In both cases, phase separation occurs between an oxygen-rich *Fmmm* phase and a nearly stoichiometric *Bmab* phase. The $La_2NiO_{4+\delta}$ system, however, exhibits a much larger solubility for excess oxygen and does not require high oxygen pressures to obtain single-phase *Fmmm* samples. Thus, in the present study we have been able to synthesize a single-phase sample with excess oxygen and refine the structure of the interstitial oxygen defect.

In the case of $La_2CuO_{4+\delta}$, temperature-dependent diffraction studies above and below room temperature showed that the phase separation occurred reversibly near room temperature, leading to the remarkable conclusion that significant oxygen diffusion was occurring near room temperature. In the present study, which focuses on the structure of the defect rather than the details of the phase diagram, we have not extended our measurements above room temperature. Thus, we are not able to state the temperature at which the phase separation begins or comment on the rate at which oxygen diffusion occurs near room temperature. We did observe,

however, that a sample of initial composition $La_2CuO_{4.00}$ readily changes its bulk oxygen content [as determined by thermogravimetric analysis (TGA) and neutron powder diffraction] if exposed to air for several days at room temperature. Thus, significant oxygen diffusion near room temperature may also be possible in $La_2NiO_{4+\delta}$.

Despite these similarities in the $La_2CuO_{4+\delta}$ and $La_2NiO_{4+\delta}$ compounds, it is important to realize that the quantitative details of the phase diagrams may not be identical. In particular, the location and shape of the miscibility gap may not be the same. For example, it appears that the phase separation occurs at higher temperatures in the Ni compound than in the Cu compound. Additionally, in the Ni compound, the oxygen content in the *Fmmm* phase of a two-phase sample is near $\delta=0.13$, while in the Cu compound, the most recent work yields a value near $\delta=0.18-0.10$.[31,32] In the case of superconducting $La_2CuO_{4+\delta}$, these differences, although small, can have a dramatic effect on the superconducting behavior, since T_c can depend critically on the number of carriers.[33] Thus, future studies of the phase diagrams of these compounds should focus on a more quantitative determination of the phase boundaries.

Although it is not proven, the remarkable similarity between the $La_2NiO_{4+\delta}$ and $La_2CuO_{4+\delta}$ systems suggests that the same defect structure, with perhaps small atom displacements to accommodate favorable interatomic distances, probably occurs in $La_2CuO_{4+\delta}$. Recent single-crystal neutron diffraction studies of $La_2CuO_{4+\delta}$ do, in fact, find a similar defect and support this assumption.[34] The formation of an oxygen interstitial (O^{2-}) defect is consistent with the occurrence of superconductivity in $La_2CuO_{4+\delta}$.[1-3] The analogy to the $La_{2-x}Sr_xCuO_4$ system is informative. Assuming that the same degree of charge transfer to the CuO_2 layers occurs in both cases, one interstitial O^{2-} defect is equivalent to two substitutional Sr^{2+} defects at the La^{3+} site. Thus, by comparison with the $La_{2-x}Sr_xCuO_4$ system where T_c is maximum for $x=0.15-0.2$,[28] the optimum superconducting properties would be expected to occur near $\delta=0.08-0.1$. Although precise stoichiometry measurements have been difficult due to superficial oxygen species,[31] this predicted optimum doping level is near that actually observed in superconducting $La_2CuO_{4+\delta}$.[1,31,32] Such agreement cannot be obtained if other defect models, i.e., superoxide or peroxide defects, are invoked to explain the superconductivity. With regard to the recent claims of superconductivity in $La_2NiO_{4+\delta}$,[6] it is interesting to note that (at least for the synthesis conditions described here) the same optimal oxygen concentration, $\delta=0.08-0.1$, may be unattainable due to the topology of the phase diagram.

ACKNOWLEDGMENTS

The authors wish to acknowledge useful discussions with B. Morosin, and with M. Marezio, who was willing to discuss unpublished structural results for $La_2CuO_{4+\delta}$ while the present work was in progress.[34] The authors also thank J. M. Honig, whose recent report of superconductivity in $La_2NiO_{4+\delta}$ (Ref. 6) motivated us to raise the priority of our ongoing studies of this system. This work is supported by the U.S. Department of Energy, Basic Energy Sciences–Materials Sciences, under Contract No. W-31-109-ENG-38. One of us (D.R.R.) would like to thank American Air Liquide, Inc. for support.

[1] J. D. Jorgensen, B. Dabrowski, Shiyou Pei, D. G. Hinks, L. Soderholm, B. Morosin, J. E. Shirber, E. L. Venturini, and D. S. Ginley, Phys. Rev. B **38**, 11337 (1988).

[2] J. Beille, B. Chevalier, G. Demazeau, F. Deslandes, J. Etourneau, O. Laborde, C. Michel, P. Lejay, J. Provost, B. Raveau, A. Sulpice, J. L. Tholence, and R. Tournier, Physica B **146**, 307 (1987).

[3] J. D. Schirber, B. Morosin, R. M. Merrill, P. F. Hlava, E. L. Venturini, J. F. Kwak, P. J. Nigrey, R. J. Baughman, and D. S. Ginley, Physica C **152**, 121 (1988).

[4] D. J. Buttrey, P. Ganguly, J. M. Honig, C. N. R. Rao, R. R. Schartman, and G. N. Subbanna, J. Solid State Chem. **74**, 233 (1988).

[5] D. J. Buttrey, H. R. Harrison, J. M. Honig, and R. R. Schartman, J. Solid State Chem. **54**, 407 (1984).

[6] Z. Kakol, J. Spalek, and J. M. Honig, J. Solid State Chem. (to be published).

[7] J. D. Jorgensen, J. Faber, Jr., J. M. Carpenter, R. K. Crawford, J. R. Haumann, R. L. Hitterman, R. Kleb, G. E. Ostrowski, R. J. Rotella, and T. G. Worlton, J. Appl. Crystallogr. (to be published).

[8] R. B. Von Dreele, J. D. Jorgensen, and C. G. Windsor, J. Appl. Crystallogr. **15**, 581 (1982).

[9] J. B. Goodenough and S. Ramasaesha, Mater. Res. Bull. **17**, 383 (1982).

[10] A. Rabenau and P. Eckerlin, Acta Crystallogr. **11**, 304 (1958).

[11] H. Muller-Buschbaum and U. Lehman, Z. Anorg. Allg. Chem. **447**, 47 (1978).

[12] P. Odier, M. Leblanc, and J. Choisnet, Mater. Res. Bull. **21**, 787 (1986).

[13] J. Rodriguez-Carvajal, J. L. Martinez, J. Pannetier, and R. Saez-Puche, Phys. Rev. B **38**, 7148 (1988).

[14] P. Odier, Y. Nigara, J. Coutures, and M. Sayer, J. Solid State Chem. **56**, 32 (1985).

[15] C. N. R. Rao, D. J. Buttrey, N. Otsuka, P. Ganguly, H. R. Harrison, C. J. Sandberg, and J. M. Honig, J. Solid State Chem. **51**, 266 (1984).

[16] R. A. Mohan Ram, L. Ganapathi, P. Ganguly, and C. N. R. Rao, J. Solid State Chem. **63**, 139 (1986).

[17] B. Grande, H. Muller-Buschbaum, and M. Schweizer, Z. Anorg. Allg. Chem. **428**, 120 (1977).

[18] U. Lehmann and H. R. Muller-Buschbaum, Z. Anorg. Allg. Chem. **470**, 59 (1980).

[19] P. Ganguly and C. N. R. Rao, J. Solid State Chem. **53**, 193 (1984).

[20] P. Ganguly, in *Advances in Solid State Chemistry,* edited by C. N. R. Rao (Indian National Science Academy, New Delhi, 1986), p. 135.

[21] J. D. Jorgensen *et al.* (unpublished).

[22] T. Egami, W. Dmowski, J. D. Jorgensen, D. G. Hinks, D. W. Capone II, C. U. Segre, and K. Zhang, *Reviews of Solid State Science* (World Scientific, Singapore, 1987), Vol. 1, No. 2, pp.

247–257.
[23]D. McK. Paul, G. Balakrishnan, N. R. Bernhoeft, W. I. F. David, and W. T. A. Harrison, Phys. Rev. Lett. **58**, 1976 (1987).
[24]D. E. Cox, S. C. Moss, R. L. Meng, P. H. Hor, and C. W. Chu, J. Mater. Res. **3**, 1327 (1988).
[25]J. D. Axe, D. E. Cox, K. Mohanty, H. Moudden, A. R. Moodenbaugh, Y. Xu, and T. R. Thurston, IBM J. Res. Dev. (to be published); J. D. Axe, A. H. Moudden, D. Hohlwein, D. E. Cox, K. M. Mohanty, A. R. Moodenbaugh, and Youwen Xu (submitted to Phys. Rev. Lett.).
[26]R. M. Flemming, B. Batlogg, R. J. Cava, and E. A. Rietman, Phys. Rev. B **35**, 7191 (1987).
[27]R. J. Birgeneau, C. Y. Chen, D. R. Gabbe, H. P. Jenssen, M. A. Kastner, C. J. Peters, P. J. Picone, T. Thio, T. R. Thurston, H. L. Tuller, J. D. Axe, P. Boni, and G. Shirane, Phys. Rev. Lett. **59**, 1329 (1987).
[28]P. Boni, J. D. Axe, G. Shirane, R. J. Birgeneau, C. Y. Chen, D. R. Gabbe, H. P. Jenssen, M. A. Kastner, C. J. Peters, P. J. Picone, T. Thio, and T. R. Thurston, Phys. Rev. B **38**, 185 (1988).
[29]R. J. Cava, B. Batlogg, K. M. Rabe, E. A. Rietman, P. K. Gallagher, and L. W. Rupp, Jr., Physica C **156**, 523 (1988).
[30]J. W. Rogers, Jr., N. D. Shinn, J. E. Schirber, E. L. Venturini, D. S. Ginley, and B. Morosin, Phys. Rev. B **38**, 5021 (1988).
[31]J. Zhou, S. Sinha, and J. B. Goodenough, Phys. Rev. B **39**, 12331 (1989).
[32]B. Dabrowski, J. D. Jorgensen, D. G. Hinks, D. R. Richards, H. B. Vanfleet, and D. L. Decker (unpublished).
[33]J. B. Torrance, Y. Tokura, A. I. Nazzal, A. Bezinge, T. C. Huang, and S. S. P. Parkin, Phys. Rev. Lett. **61**, 1127 (1988).
[34]C. Chaillout, S. W. Cheong, Z. Fisk, M. S. Lehmann, M. Marezio, B. Morosin, and J. E. Schirber, Physica C **158**, 183 (1989).